Journal of Materials Chemistry B

ROYAL SOCIETY OF CHEMISTRY

PAPER

Cite this: J. Mater. Chem. B, 2020, 8, 3647

Flexible and stretchable dual mode nanogenerator for rehabilitation monitoring and information interaction†

Zhuo Liu,[ab] Qiang Zheng,[bc] Yue Shi,[bd] Lingling Xu,[bc] Yang Zou,[bc] Dongjie Jiang,[bc] Bojing Shi,[ab] Xuecheng Qu,[bc] Hu Li,[ab] Han Ouyang,[ab] Ruping Liu,[bd] Yuxiang Wu,*[e] Yubo Fan*[af] and Zhou Li *[bc]

Received 4th November 2019,
Accepted 14th January 2020

DOI: 10.1039/c9tb02466b

rsc.li/materials-b

Motion recognition and information interaction sensors with flexibility and stretchability are key functional modules as interactive media between the mechanical motions and electric signals in an intelligent robotic and rehabilitation training system. Nanogenerators have many useful applications in the field of intelligent interaction, with the advantages of a self-powered sensing ability, easy fabrication, considerable sensitivity and reliability. However, the singularity of the sensing mode limits its applications. Hence, in this research, a flexible and stretchable dual mode nanogenerator (FSDM-NG) for human motion sensing and information interaction, based on the integration of piezoelectric and triboelectric principles was developed. In piezoelectric mode, the FSDM-NG can effectively monitor the bending angle of joints (finger, wrist and elbow) from 30° to 90°. In triboelectric mode, text and logic information transfer are encoded using Morse code and logic gates, respectively. In addition, the device has good adhesion and biosafety, and is robust which makes it work normally even in under water environments. Combining these two sensing mechanisms, multiple modes of sensing from touch and stretch based on the FSDM-NG can be achieved for information interaction in real time. The proposed sensor has the potential to be adapted for more complex sensing, which may provide new applications for intelligent interaction of robots and in the rehabilitation training field.

Introduction

The application of flexible and portable electronic medical devices in clinical medicine and daily monitoring have attracted great attention, and include heart rate sensors,[1,2] blood pressure sensors,[3–5] respiration sensors,[6–9] limb motion sensors[10–13] and so on. In the rehabilitation process for dyskinesia, limb motion monitoring is critical for showing the patient's current recovery status and to assess their physiological function. In addition, there are some special patients who are unable to communicate normally with others, especially the medical staff, which poses great challenges for correctly guiding the rehabilitation process. Therefore, a man–machine interaction interface that establishes connections between patients, doctors, and medical devices is essential. In recent years, the research on the man–machine interaction interface has become more and more popular with the rapid development of artificial intelligence (AI).[14–20] The application of AI has now gone deep into every aspect of life as well as in the modern medical system. One of the most important research directions in this area is the design of a portable man–machine interaction interface fitted to the body, for establishing multiple, intelligent and effective contact pathways between users and devices,[21–24] which is of great significance for solving the problems of communication and guidance in some special medical cases, as mentioned previously. Moreover, current diversified sensors of information interaction and motion are dependent on the batteries that need regular

[a] Beijing Advanced Innovation Centre for Biomedical Engineering, Key Laboratory for Biomechanics and Mechanobiology of Ministry of Education, School of Biological Science and Medical Engineering, Beihang University, Beijing 100083, China. E-mail: yubofan@buaa.edu.cn
[b] CAS Center for Excellence in Nanoscience, Beijing Key Laboratory of Micro-nano Energy and Sensor, Beijing Institute of Nanoenergy and Nanosystems, Chinese Academy of Sciences, Beijing 100083, China. E-mail: zli@binn.cas.cn
[c] School of Nanoscience and Technology, University of Chinese Academy of Sciences, Beijing 100049, China
[d] School of Printing and Packaging Engineering, Beijing Institute of Graphic Communication, Beijing 102600, China
[e] School of Physical Education, Jianghan University, Wuhan 430056, China. E-mail: yxwu@jhun.edu.cn
[f] Key Laboratory of Human Motion Analysis and Rehabilitation Technology of the Ministry of Civil Affairs, National Research Center for Rehabilitation Technical Aids, Beijing 100176, China

† Electronic supplementary information (ESI) available. See DOI: 10.1039/c9tb02466b

replacing or charging which greatly limits their applications. Hence, a versatile device capable of both self-powered limb monitoring and information interaction will be of great value for future applications.

Recent developments in nanogenerator technology have shown good progress in solving the previously mentioned issues.[25–30] The triboelectric nanogenerator and piezoelectric nanogenerator can convert mechanical energy into electricity which can also be a self-powered sensor (pressure sensors,[31–33] tactile sensors,[34–36] sound sensors,[37,38] implantable medical sensors,[39–41] biosensors,[42,43] and for message transfer[44] and so on) with advantages of light weight, low cost, high conversion efficiency and easy fabrication.[45] A poly(vinylidene fluoride) (PVDF) based piezoelectric nanogenerators has attracted attention because of its outstanding piezoelectric property with β-phase piezoelectric crystallization.[46] Recent papers in the literature have included work on PVDF composites to further adjust the properties of the PVDF, such as BNBT-PVDF,[47] MWNTs/$BaTiO_3$/PVDF,[48] Al/PVDF[49] and so on. In addition, some studies have demonstrated a piezoelectric/triboelectric hybrid generator to enhance output performance as a power source for wearable devices.[50,51]

In the research reported here, a flexible and stretchable dual mode nanogenerator (FSDM-NG) for limb motion sensing and information interaction was developed. The FSDM-NG is fabricated from a PVDF band and silicone. The PVDF band is designed as a wave structure and inlaid in the silicone. Using the piezoelectric mechanism, the relationship between the output performances of the device and tensile length and frequency have been systematically studied. With the frequency increase from 1 Hz to 2.5 Hz, the open-circuit voltage (V_{oc}) is nearly stable with a value of ~16 V, and the short-circuit current (I_{sc}) increases from 62 nA to 175 nA. The current density of the device is about 166.7 nA cm^{-2} at 2 Hz, which is higher than the recently reported values for other PVDF based NGs.[42,52–56] The stretchability of the FSDM-NG can reach 33.33%. It is successfully demonstrated that the FSDM-NG can be comfortably and conformally attached to human joints (finger joints, wrist joints and elbow joints) to monitor the degree of bending from 30° to 90° and the bending frequency (1–2.5 Hz) based on the electrical signal of the piezoelectric nanogenerator. Under the triboelectric mechanism, with the single electrode triboelectric nanogenerator, the V_{oc}, I_{sc} and short-circuit charge (Q_{sc}) of the FSDM-NG can reach ~45 V, 150 nA and 6 nC, respectively. Interestingly, by using Morse code and logic gates, the text and logic information can be encoded by the electrical waveform by touching the surface of the FSDM-NG. This work introduces a novel method for information interaction, which has the potential to be applied in applications for a man–machine interaction interface and rehabilitation training sensing.

Experimental section

Fabrication of the FSDM-NG

Fig. S1 (ESI†) illustrates the fabrication process of the FSDM-NG. First, the mold of the wave structure was fabricated using 3D printing of poly(lactic acid) (PLA) (Raise 3D Technologies). Then the silicone (Smooth-On, Inc.) consisting of Part A and Part B was dispensed into a mixing container in a ratio of 1 : 1 by weight. After mixing thoroughly for 3 min, the mixture was placed in a vacuum drying chamber (DXG-9073B1) for 3 minutes to remove bubbles. The mixture within the container was cured at 50 °C for 2 h. After curing, the silica gel was carefully peeled off from the molds, and a concave wave shape was formed in the silica gel. The PVDF film was cut with scissors to obtain the PVDF band with a thinness of 1 mm, and the electrodes were fixed on both sides to enameled wire. The PVDF band was inlaid in a silicone wavy groove, then packaged by prepared silica gel.

Characterization and measurement

A linear motor (LinMot, E1100) was employed to pull the FSDM-NG, and different tensile frequencies were achieved by adjusting the displacement, velocity, acceleration and displacement of the linear motor. A Keithley 6517 electrometer was used for measuring the V_{oc}, I_{sc}, Q_{sc} of the FSDM-NG, and the data were recorded and collected by an oscilloscope (LeCroy, HDO6104). The piezoelectric constant (d_{33}) of the PVDF was measured by a quasi-static d_{33} measuring instrument (ZJ-4AN, Institute of Acoustics, Chinese Academy of Science, Beijing, China). The microscopic images of the PVDF band were characterized by a Hitachi SU8020 scanning electron microscope. Fourier transformation infrared (FTIR) spectrometry analysis was performed using a Bruker Vertex 80V.

Results and discussion

Overview of the limb sensing and information interaction system

Fig. 1a, shows the limb sensing and information interaction system based on the FSDM-NGs with different working modes to realize limb motion monitoring (d_{31} mode of piezoelectric nanogenerator) and information interaction (single electrode mode of triboelectric nanogenerator). The d_{31} mode that the piezoelectric material is subjected to, is a force perpendicular to the direction of the polarization electric field (Fig. S2, ESI†). The PVDF band with the Ag electrode is inlaid in the silicone, and this constitutes the FSDM-NG (Fig. 1b). The breadth and thinness of the PVDF band were about 1 mm and 110 μm, respectively. The diameter of single semicircle was about 1.5 cm. The length could be adjusted according to the actual situation, and the detailed fabrication process is presented in the Materials and methods section. The surface and cross-section microstructure of the PVDF band is shown in Fig. S3 (ESI†). The β-phase piezoelectric structure of the PVDF band was also demonstrated by FTIR measurements (Fig. S4, ESI†). The working principle of piezoelectric effect of the FSDM-NG is shown in Fig. 1c. In detail, because of the positive piezoelectric effect of the PVDF band, the device could convert the mechanical energy to the electricity. When a periodic mechanical force was applied in the direction of the vertical device by pulling the

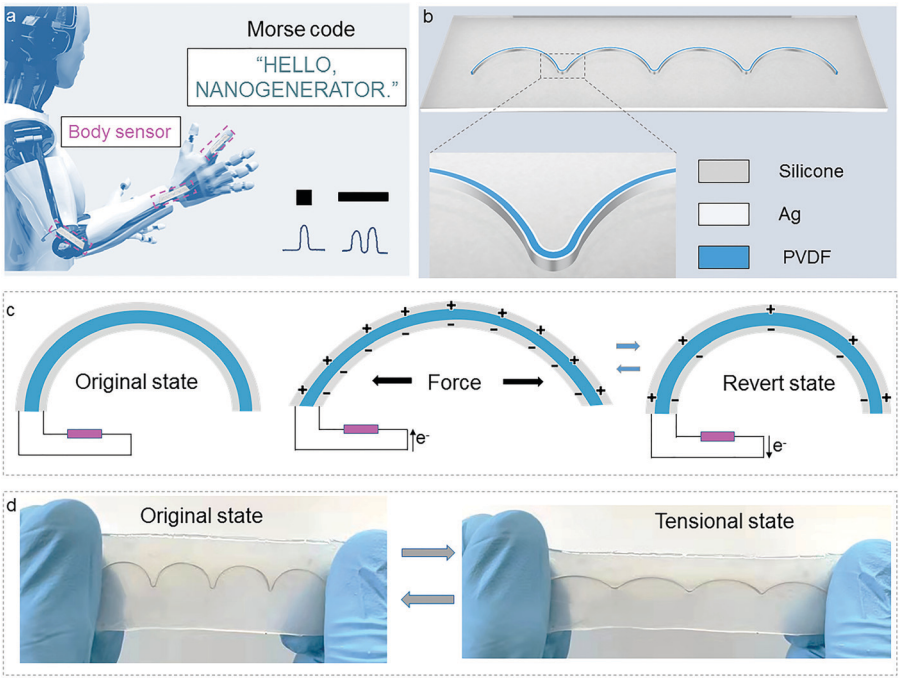

Fig. 1 Overview of the limb sensing and information interaction system. (a) The limb sensing and information interaction system consisted of multiple FSDM-NGs to realize the different functions. (b) Schematic diagram of the FSDM-NG. (c) Working principle of the d_{31} mode of the piezoelectric nanogenerator from the FSDM-NG. (d) Photographs of the FSDM-NG under original and tensional states.

silicone, the PVDF band generated piezoelectric polarization charges and an electric field to prompt the circular electron flow from one electrode to the other electrode. Ultra-soft silicone was employed as the elastomeric dielectric and encapsulation layer, because of its robust mechanical properties, biocompatibility and excellent flexibility/stretchability. As shown in Fig. 1d, the FSDM-NG can be stretched along the in-plane direction of the wave structure. The good stretchability of the whole device was attributed to the ingenious design of the wave structure for the PVDF band. When the FSDM-NG was stretched by the external tensile stress, the wave structure of the PVDF was gradually straightened and the silicone gradually extended along the direction of the tensile stress to adapt to the external loading. The stretchability of the FSDM-NG depended on the diameter (d) and altitude (h) of the wave structure for the PVDF band and the thickness (l) of the silicone. In this work, the d, h and l were about 1.5 cm, 0.75 cm and 2 mm, respectively. In reality, the relevant parameters (d, h and l) can be adjusted for different practical applications.

Electrical output performance characterization of the FSDM-NG under the piezoelectric mechanism

Due to its excellent flexibility and stretchability, the FSDM-NG can be freely twisted without any mechanical failure (Fig. 2a). The stretch rate of the FSDM-NG can reach 33.33% (Fig. 2b), which was effective for limb monitoring. The tensile frequency response of the FSDM-NG was demonstrated under the piezoelectric nanogenerator mode (Fig. 2c–f). The piezoelectric constant (d_{33}) value of the PVDF was about 19 pC N^{-1}. When the FSDM-NG was stretched by a linear motor at frequencies ranging from 1 Hz to 2.5 Hz, the V_{oc} and the Q_{sc} were stable around 16 V and 8.8 nC, respectively (Fig. S5, ESI†). Meanwhile, the I_{sc} increased from 62 nA to 175 nA (Fig. 2g–j). The current density of the device was about 166.7 nA cm^{-2} at 2 Hz, which was higher than the recently reported values for other PVDF-based NGs[42,52–56] (Table S1, ESI†). The results of the statistical analysis of the relationship between V_{oc}, I_{sc} and frequency are shown in Fig. 2k and l, respectively. Based on the previous results, in the low frequency state that satisfied the change in the frequency of limb movement, the I_{sc} of the FSDM-NG was positively correlated with the tensile frequency. The relationship between the V_{oc} and the different stretched lengths of the FSDM-NG were also explored (Fig. 2m). The V_{oc} was about 16 V under normal status with a 25% strain rate. The results showed that the V_{oc} of the FSDM-NG increased nearly one-fold as the strain increased from 25% to 30%. This was because the V_{oc} was proportional to the stress. Based on the d_{31} mode of the piezoelectric nanogenerator, the V_{oc} can be defined as:

$$V_{oc} = \sigma_1 g_{31} H \quad (1)$$

where, H is the thickness of the piezoelectric layer, σ_1 is the stress in the 1 direction, and g_{31} is the strain constant. After 5000 mechanical stimuli cycles by linear motor, the V_{oc} of the device was maintained stably at about 16 V when compared with its initial state, and the surface of the device showed no damage, and exhibited outstanding durability and stability (Fig. S6, ESI†). The outputs of the device at different load resistances are shown in Fig. S7 (ESI†). The power can reach

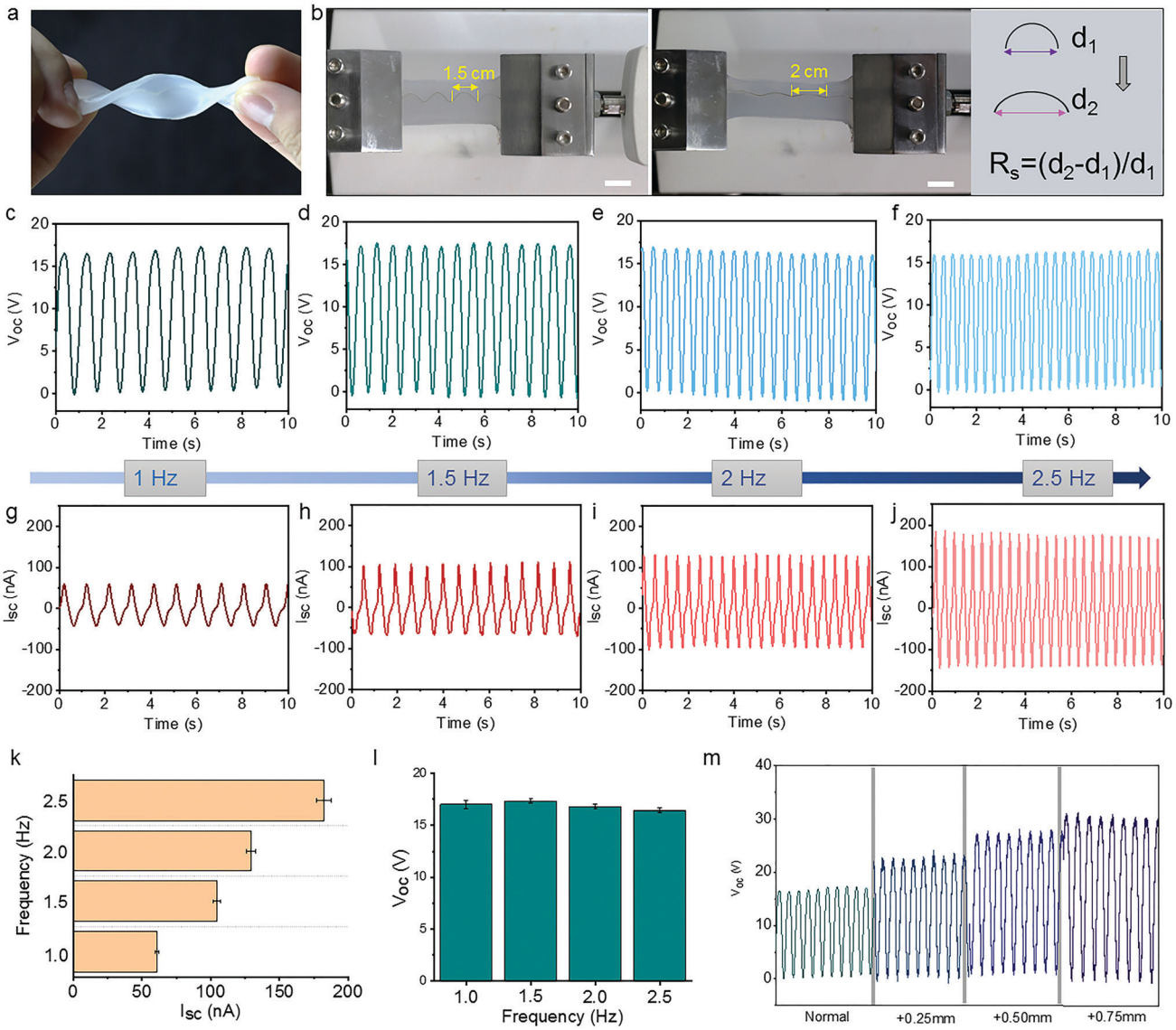

Fig. 2 Electrical output performance characterization of the FSDM-NG under a piezoelectric mechanism. (a) Photograph of FSDM-NG under b twisting. (b) Photographs of FSDM-NG without stretch (right) and while stretched to 33.33% (left), scale bar = 1 cm. (c–f) V_{oc}, and (g–j) I_{sc} of the FSDM-NG under different loading frequencies from 1 Hz to 2.5 Hz. (k and l) Statistical analysis for I_{sc} and V_{oc} of the FSDM-NG with different stimulation frequencies. (m) V_{oc} of the FSDM-NG under different tensile elongation.

up to ~490 nW, and the typical internal resistance of the device was ~200 MΩ.

Limb motion sensing based on the FSDM-NG under a piezoelectric mechanism

Because of the good stretching capacity and electrical output performance of the FSDM-NG, it can be employed as a wearable self-powered sensor to monitor limb movement, which may be useful for developing intelligent robot sensing and rehabilitation monitoring. As demonstrated in Fig. 3a–c, the FSDM-NG was attached to the finger joints, wrist joints and elbow joints, respectively. The I_{sc} signal of the device responded to a small amount of bending of the limb. Four different bending angles were monitored on these three joints. Taking the finger joints as an example, the top and bottom of the device were fixed, and the FSDM-NG was stretched as the bending angle increased, and the larger the bending angle of the finger, the longer the FSDM-NG was stretched. The finger with 30°, 45°, 60° and 90° degrees of bending are characterized from left to right in Fig. 3a. It was observed that the electric outputs of FSDM-NG increased correspondingly, together with the bending trend of the finger from 30° to 90°. This phenomenon was also confirmed with the wrist joints and elbow joints, and was because of the enhancement of stress and strain. The bending frequency monitoring by the device was also investigated. As shown in Fig. 3d, when increasing the bending frequency per unit time with the same bending angle at 45°, the electric outputs of FSDM-NG were obviously positively correlated with the bending frequency. Fig. 3e and f demonstrate the monitoring process of grasping one object (a cup) *via*

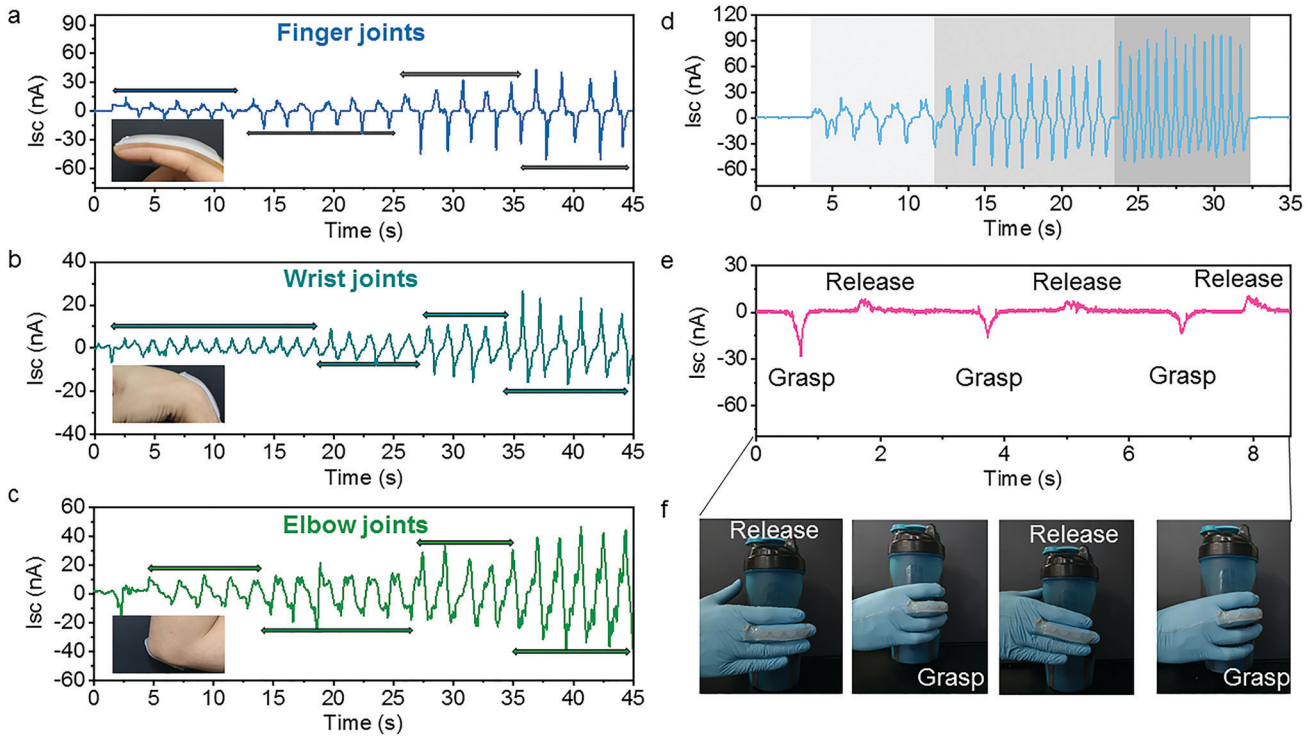

Fig. 3 Limb motion sensing based on the FSDM-NG under a piezoelectric mechanism. (a–c) Monitoring the bending amplitude of joints including finger joints, wrist joints and elbow joints. (d) I_{sc} of the FSDM-NG under different bending frequencies while they were attached onto the finger. (e) Monitoring limb motion while grasping the cup, and (f) photographs of the different status of limb motion corresponding to (e).

the FSDM-NG. The FSDM-NG still maintained good output performance under water (Fig. S8 and Video S1, ESI†). This application may play important role in robot control and rehabilitation training for people with disabilities in the future.

Output performance characterization of the FSDM-NG under a triboelectric mechanism

The device has excellent tensile properties in the horizontal direction, and the single-electrode mode of the FSDM-NG in the vertical direction also has fascinating features. As shown in Fig. 4a, a linear motor was employed to explore the output performance of the FSDM-NG under a single electrode based on a triboelectric nanogenerator. Nitrile rubber was placed onto the top of the linear motor as the triboelectric layer, so that it touched the surface of the FSDM-NG, during the testing so that one of the two electrodes was able to make a connection. The working principle of the FSDM-NG is shown in Fig. 4b, when the nitrile rubber came into contact with the surface of the FSDM-NG, the nitrile rubber had a lower electron affinity than silica gel, and therefore, the electrons were injected into the silicone based on the triboelectric effect. The negative triboelectric charges were retained on the surface of the silicone for long time because they are high-molecular polymer materials. Because of the electrostatic effect, when the nitrile rubber with a positive charge approached the surface of silicone, the electric potential of the Ag electrode changed, which resulted in electron flow from the ground to the Ag electrode under a short-circuit condition. When the nitrile rubber was completely connected to the silicone, the transferred charges from the ground to the Ag electrode will reach maximum values as will the electric potential of the Ag electrode. When the nitrile rubber was separated from the silicone, the electric potential of the Ag electrode will recover gradually, which caused electrons to flow back to the ground. Then, as the nitrile rubber goes back to its initial position, the triboelectric charge distribution of the FSDM-NG returns to its initial state. The reciprocating, flowing electrons will form alternating current between the Ag electrode and the ground. In addition, periodic contact and separation between the nitrile rubber and silicone will produce a continuous alternating current signal. The output performance of the FSDM-NG under the single-electrode mode of the triboelectric nanogenerator are shown in Fig. 4c–e. When the FSDM-NG was touched by a nitrile rubber film with a size of 2.5 cm × 4 cm at a frequency of about 1 Hz, the V_{oc}, I_{sc} and Q_{sc} can reach ~45 V, 150 nA and 6 nC, respectively.

Information interaction of the FSDM-NG under a triboelectric mechanism

The single-electrode FSDM-NG based on the triboelectric nanogenerator, which simplified the structure of the double electrode mode of the triboelectric nanogenerator and greatly expanded the possible application scenarios of the device for information interaction. In the field of telecommunications, Morse code is used for encoding text based on the two different signal durations (dots and dashes). The 26 English letters, Arabic numerals and some specific symbols can be represented by Morse code *via*

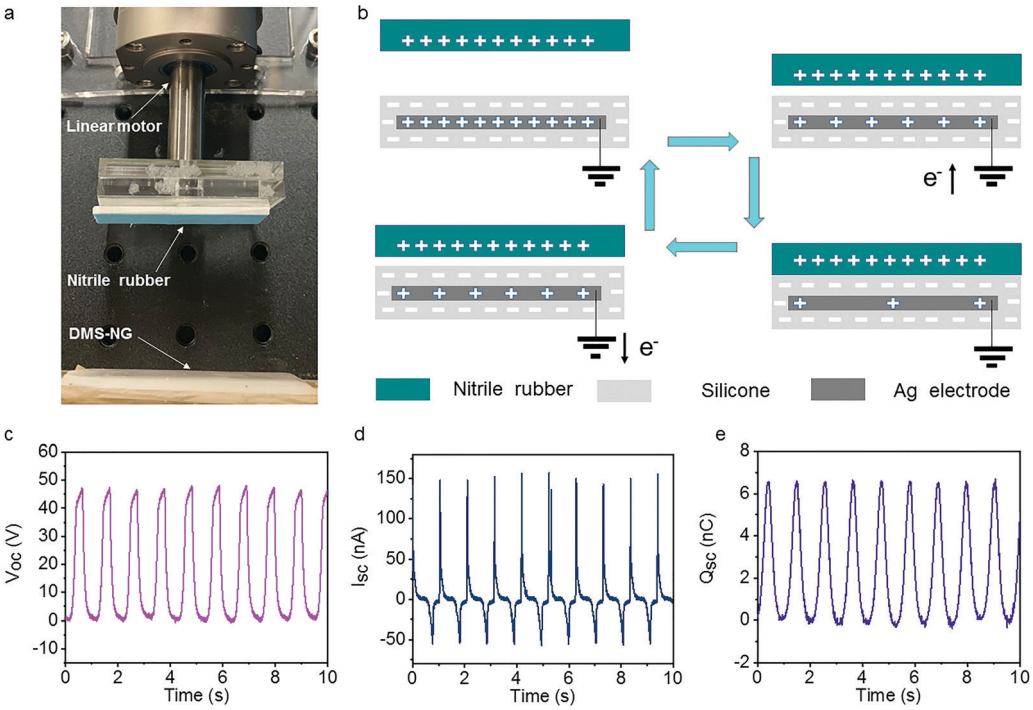

Fig. 4 Output performance characterization of the FSDM-NG under a triboelectric mechanism. (a) Photograph of the single electrode test system. (b) Working principle with a single electrode FSDM-NG. (c–e) V_{oc}, I_{sc}, and Q_{sc} of the FSDM-NG driven by the linear motor.

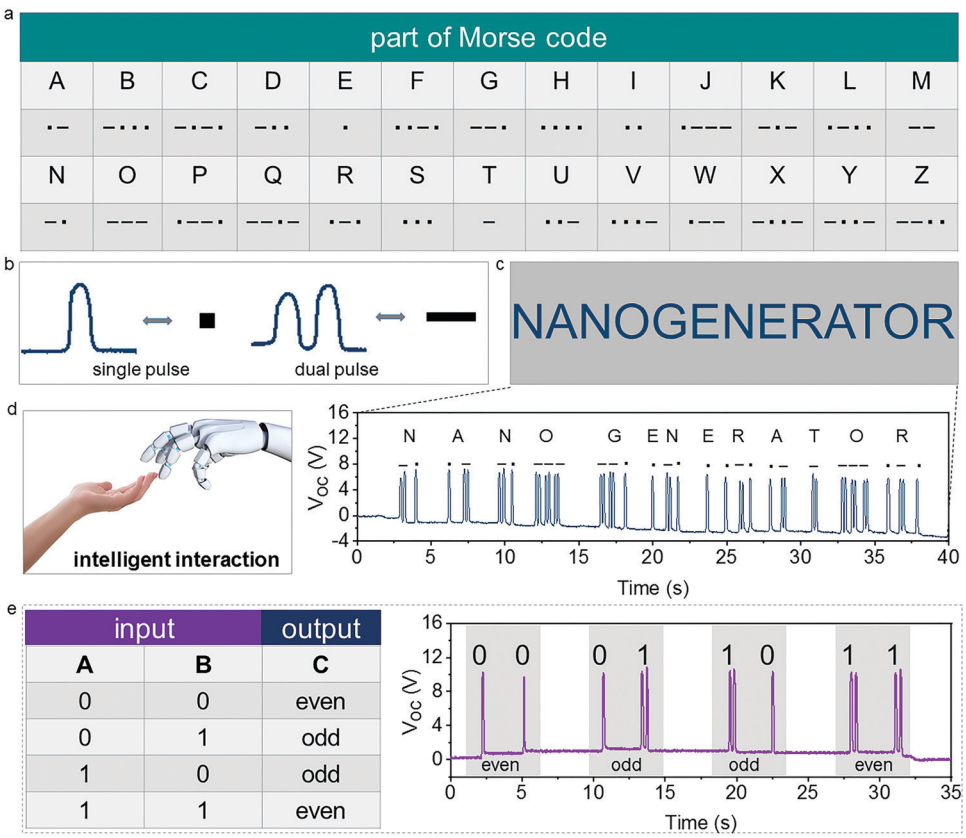

Fig. 5 Information interaction of the FSDM-NG under a triboelectric mechanism. (a) Part of Morse code. (b) Relationship between the output signal of the FSDM-NG and the input signal of Morse code. (c) Demonstration of the information interaction with the output signal of the FSDM-NG based on the Morse code. (d) Schematic diagram of a man–machine interactive system. (e) Custom table of the logic signal and relationship between the output signal of the FSDM-NG and the input signal of the logical gate.

unique combinations of dots and dashes. In this work, the single-electrode mode of the FSDM-NG can be also employed to deliver information. Fig. 5a shows a part of Morse code including 26 English letters. A single pulse from the FSDM-NG by contacting the surface once was defined as a dot in Morse code, and a dual pulse was defined as a dash (Fig. 5b). As illustrated in Fig. 5c, according the Morse code and predefined rules, the word ''NANOGENERATOR'' was encoded by the voltage signals from the FSDM-NG. To better recognize the information, when a finger touches the surface of the device continuously to deliver the information (word or sentence, Fig. 5d), it was preferred that the distance between the letters was greater than the distance between the symbols (dots and dashes). In addition, the encoding of other word was also implemented (Fig. S9 and Video S2, ESI†).

Based on the previous ideas, the single-electrode mode of the FSDM-NG was able to convert physical contact directly into electrical signals, which can also be applied using a logic gate. Analogously, the single pulse and dual pulse were defined as ''0'' and ''1'', respectively. The combinations of single and double pulse signals can construct a logical relationship. For example, the relationship between input and output is defined in Fig. 5e, and simple information (even and odd) can be expressed by signals generated by touching the surface of the FSDM-NG. Certainly, ''0'' and ''1'' can be also represent ''yes'' and ''no'' for simple response communication, based on the logical definition, ''0 1'' or ''1 0'' can be used to express ''uncertainty'', and in contrast, ''1 1'' and ''0 0'' can be used to express ''yes'' and ''no'', respectively. Furthermore, in practice based on a logic gate, more complex logic can also be defined for information interaction and cryptography.

Conclusions

In summary, a novel structural sensor with advantages of flexibility, stretchability and biosecurity, is proposed, which integrated two sensing mechanisms – piezoelectric and triboelectric for monitoring limb movement and information interaction. Under the piezoelectric mechanism, the wave structure PVDF band with a width of 1 mm is inlaid into super soft silicone. It can be comfortably attached onto joints to monitor limb movement (bending degree and bending frequency) *via* the value of the electrical signal. Certainly, the joint's angular position can be identified based on the value of the electrical signal from the device. When the FSDM-NG is attached on the finger, the action of grasping a cup with the hand can be recorded well. These applications have great potential for use in robotic motion learning and rehabilitation training. Compared with the excellent tensile properties of the piezoelectric mechanism in the horizontal direction, the triboelectric mechanism can achieve information transfer by contact and separation of triboelectric layers in the vertical direction. Under the single-electrode triboelectric nanogenerator, one of the two electrodes of the FSDM-NG are employed to connect. By customizing the relationship between the electrical waveform characteristics of the FSDM-NG and Morse code (dots and dashes), a variety of text can be encoded. In the demonstration, the word ''NANOGENERATOR'' is transmitted by the FSDM-NG. Moreover, the relationship between the waveform characteristics of the FSDM-NG and the logic gates is also defined in a similar way. A similar decision can be achieved through a custom logical operation relationship. Information interaction plays an extremely important role in intelligent robots, and this method that is proposed may open up a new way of thinking. If these two sensing mechanisms are combined, multiple modes of sensing from touch and stretch based on one device can also be achieved. In the future, the size and structure of the device will be further optimized, and integrated with a backend module. The FSDM-NG could be used for more complex motion monitoring and information interaction in the field of rehabilitation training and intelligent robotics.

Conflicts of interest

There are no conflicts to declare.

Acknowledgements

This study was supported by the National Key R&D project from Ministry of Science and Technology, China (2016YFA0202703), the National Natural Science Foundation of China (No. 61875015, 21801019, 11421202, 11827803 and 61971049), the 111 Project (Project No. B13003), the Beijing Natural Science Foundation (7204275), the National Postdoctoral Program for Innovative Talent (No. BX20190026), the Wuhan Municipal Science and Technology Bureau (Grant No. 2017060201010166) and the National Youth Talent Support Program. We also thank Chan Wang and Chenchen Wang for helpful discussions and assistance in the experiments.

References

1 Y. H. Kwak, W. Kim, K. B. Park, K. Kim and S. Seo, *Biosens. Bioelectron.*, 2017, **94**, 250–255.
2 S. W. Kim, S. B. Choi, Y.-J. An, B.-H. Kim, D. W. Kim and J.-G. Yook, *IEEE Trans. Biomed. Eng.*, 2015, **62**, 2568–2575.
3 N. Luo, W. Dai, C. Li, Z. Zhou, L. Lu, C. C. Poon, S. C. Chen, Y. Zhang and N. Zhao, *Adv. Funct. Mater.*, 2016, **26**, 1178–1187.
4 G. Schwartz, B. C.-K. Tee, J. Mei, A. L. Appleton, D. H. Kim, H. Wang and Z. Bao, *Nat. Commun.*, 2013, **4**, 1859.
5 Y. Pang, H. Tian, L. Tao, Y. Li, X. Wang, N. Deng, Y. Yang and T.-L. Ren, *ACS Appl. Mater. Interfaces*, 2016, **8**, 26458–26462.
6 S. Kano, K. Kim and M. Fujii, *ACS Sens.*, 2017, **2**, 828–833.
7 Z. Liu, S. Zhang, Y. Jin, H. Ouyang, Y. Zou, X. Wang, L. Xie and Z. Li, *Semicond. Sci. Technol.*, 2017, **32**, 064004.
8 K. Takei, W. Honda, S. Harada, T. Arie and S. Akita, *Adv. Healthcare Mater.*, 2015, **4**, 487–500.
9 H. Zhang, J. Zhang, Z. Hu, L. Quan, L. Shi, J. Chen, W. Xuan, Z. Zhang, S. Dong and J. Luo, *Nano Energy*, 2019, **59**, 75–83.

10 G. Ge, Y. Zhang, J. Shao, W. Wang, W. Si, W. Huang and X. Dong, *Adv. Funct. Mater.*, 2018, **28**, 1802576.
11 Y. Yamamoto, S. Harada, D. Yamamoto, W. Honda, T. Arie, S. Akita and K. Takei, *Sci. Adv.*, 2016, **2**, e1601473.
12 Z. Wang, S. Wang, J. Zeng, X. Ren, A. J. Chee, B. Y. Yiu, W. C. Chung, Y. Yang, A. C. Yu and R. C. Roberts, *Small*, 2016, **12**, 3827–3836.
13 L. Guan, S. Yan, X. Liu, X. Li and G. Gao, *J. Mater. Chem. B*, 2019, **7**, 5230–5236.
14 L. Dhakar, P. Pitchappa, F. E. H. Tay and C. Lee, *Nano Energy*, 2016, **19**, 532–540.
15 B. Mosadegh, P. Polygerinos, C. Keplinger, S. Wennstedt, R. F. Shepherd, U. Gupta, J. Shim, K. Bertoldi, C. J. Walsh and G. M. Whitesides, *Adv. Funct. Mater.*, 2014, **24**, 2163–2170.
16 T. Someya, T. Sekitani, S. Iba, Y. Kato, H. Kawaguchi and T. Sakurai, *Proc. Natl. Acad. Sci. U. S. A.*, 2004, **101**, 9966–9970.
17 C. Wang, D. Hwang, Z. Yu, K. Takei, J. Park, T. Chen, B. Ma and A. Javey, *Nat. Mater.*, 2013, **12**, 899.
18 H.-H. Chou, A. Nguyen, A. Chortos, J. W. To, C. Lu, J. Mei, T. Kurosawa, W.-G. Bae, J. B.-H. Tok and Z. Bao, *Nat. Commun.*, 2015, **6**, 8011.
19 X. Wang, L. Dong, H. Zhang, R. Yu, C. Pan and Z. L. Wang, *Adv. Sci.*, 2015, **2**, 1500169.
20 A. Chortos, J. Liu and Z. Bao, *Nat. Mater.*, 2016, **15**, 937.
21 A. P. Gerratt, H. O. Michaud and S. P. Lacour, *Adv. Funct. Mater.*, 2015, **25**, 2287–2295.
22 M. Park, Y. J. Park, X. Chen, Y. K. Park, M. S. Kim and J. H. Ahn, *Adv. Mater.*, 2016, **28**, 2556–2562.
23 C. Hou, H. Wang, Q. Zhang, Y. Li and M. Zhu, *Adv. Mater.*, 2014, **26**, 5018–5024.
24 M. Ha, S. Lim and H. Ko, *J. Mater. Chem. B*, 2018, **6**, 4043–4064.
25 Z. L. Wang and J. Song, *Science*, 2006, **312**, 242–246.
26 F.-R. Fan, Z.-Q. Tian and Z. L. Wang, *Nano Energy*, 2012, **1**, 328–334.
27 Z. Liu, H. Li, B. Shi, Y. Fan, Z. L. Wang and Z. Li, *Adv. Funct. Mater.*, 2019, **29**, 1808820.
28 J. Chen and Z. L. Wang, *Joule*, 2017, **1**, 480–521.
29 J. Briscoe and S. Dunn, *Nano Energy*, 2015, **14**, 15–29.
30 Z. L. Wang, *Mater. Today*, 2017, **20**, 74–82.
31 Q. Shi, H. Wang, T. Wang and C. Lee, *Nano Energy*, 2016, **30**, 450–459.
32 J. H. Lee, H. J. Yoon, T. Y. Kim, M. K. Gupta, J. H. Lee, W. Seung, H. Ryu and S. W. Kim, *Adv. Funct. Mater.*, 2015, **25**, 3203–3209.
33 F.-R. Fan, L. Lin, G. Zhu, W. Wu, R. Zhang and Z. L. Wang, *Nano Lett.*, 2012, **12**, 3109–3114.
34 Y. Yang, H. Zhang, Z.-H. Lin, Y. S. Zhou, Q. Jing, Y. Su, J. Yang, J. Chen, C. Hu and Z. L. Wang, *ACS Nano*, 2013, **7**, 9213–9222.
35 X. Pu, M. Liu, X. Chen, J. Sun, C. Du, Y. Zhang, J. Zhai, W. Hu and Z. L. Wang, *Sci. Adv.*, 2017, **3**, e1700015.
36 J. Park, Y. Lee, M. Ha, S. Cho and H. Ko, *J. Mater. Chem. B*, 2016, **4**, 2999–3018.
37 X. Fan, J. Chen, J. Yang, P. Bai, Z. Li and Z. L. Wang, *ACS Nano*, 2015, **9**, 4236–4243.
38 J. Yang, J. Chen, Y. Su, Q. Jing, Z. Li, F. Yi, X. Wen, Z. Wang and Z. L. Wang, *Adv. Mater.*, 2015, **27**, 1316–1326.
39 Z. Liu, Y. Ma, H. Ouyang, B. Shi, N. Li, D. Jiang, F. Xie, D. Qu, Y. Zou and Y. Huang, *Adv. Funct. Mater.*, 2019, **29**, 1807560.
40 Y. Ma, Q. Zheng, Y. Liu, B. Shi, X. Xue, W. Ji, Z. Liu, Y. Jin, Y. Zou and Z. An, *Nano Lett.*, 2016, **16**, 6042–6051.
41 Q. Zheng, H. Zhang, B. Shi, X. Xue, Z. Liu, Y. Jin, Y. Ma, Y. Zou, X. Wang and Z. An, *ACS Nano*, 2016, **10**, 6510–6518.
42 G. Khandelwal, A. Chandrasekhar, R. Pandey, N. P. M. J. Raj and S.-J. Kim, *Sens. Actuators, B*, 2019, **282**, 590–598.
43 G. Khandelwal, A. Chandrasekhar, N. P. M. J. Raj and S. J. Kim, *Adv. Energy Mater.*, 2019, **9**, 1803581.
44 A. Chandrasekhar, V. Vivekananthan, G. Khandelwal and S. J. Kim, *Nano Energy*, 2019, **60**, 850–856.
45 H. Guo, X. Pu, J. Chen, Y. Meng, M.-H. Yeh, G. Liu, Q. Tang, B. Chen, D. Liu and S. Qi, *Sci. Robot.*, 2018, **3**, eaat2516.
46 F. Liu, N. A. Hashim, Y. Liu, M. M. Abed and K. Li, *J. Membr. Sci.*, 2011, **375**, 1–27.
47 S. Hajra, S. Sahoo and R. Choudhary, *J. Polym. Res.*, 2019, **26**, 14.
48 Z.-M. Dang, L.-Z. Fan, Y. Shen and C.-W. Nan, *Mater. Sci. Eng., B*, 2003, **103**, 140–144.
49 W. Zhou, J. Zuo and W. Ren, *Composites, Part A*, 2012, **43**, 658–664.
50 W.-S. Jung, M.-G. Kang, H. G. Moon, S.-H. Baek, S.-J. Yoon, Z.-L. Wang, S.-W. Kim and C.-Y. Kang, *Sci. Rep.*, 2015, **5**, 9309.
51 X. Wang, B. Yang, J. Liu, Y. Zhu, C. Yang and Q. He, *Sci. Rep.*, 2016, **6**, 36409.
52 L. Jin, S. Ma, W. Deng, C. Yan, T. Yang, X. Chu, G. Tian, D. Xiong, J. Lu and W. Yang, *Nano Energy*, 2018, **50**, 632–638.
53 S. Siddiqui, H. B. Lee, D. I. Kim, L. T. Duy, A. Hanif and N. E. Lee, *Adv. Energy Mater.*, 2018, **8**, 1701520.
54 S. K. Karan, D. Mandal and B. B. Khatua, *Nanoscale*, 2015, **7**, 10655–10666.
55 A. Wang, Z. Liu, M. Hu, C. Wang, X. Zhang, B. Shi, Y. Fan, Y. Cui, Z. Li and K. Ren, *Nano Energy*, 2018, **43**, 63–71.
56 A. Wang, M. Hu, L. Zhou and X. Qiang, *Nanomaterials*, 2019, **9**, 349.